Original Research

Simultaneous MRI Measurement of Blood Flow, Blood Volume, and Capillary Permeability in Mammary Tumors Using Two Different Contrast Agents

Elizabeth Henderson, PhD,[1,2] Jane Sykes, RVT,[1] Dick Drost, PhD,[1] Hanns-Joachim Weinmann, PhD,[4] Brian K. Rutt, PhD,[2,3] and Ting-Yim Lee, PhD[1,2,3]*

A technique for the simultaneous measurement of three vascular parameters: blood flow ($F\rho$), blood volume (v_b), and the capillary permeability-surface area product ($PS\rho$) in breast tumors using dynamic contrast-enhanced magnetic resonance imaging (MRI) is presented. Features of the technique include measurement of precontrast tumor T_1, rapid temporal sampling, measurement of the arterial input function, and use of a distributed parameter tracer kinetic model. Parameter measurements are compared that were determined using two contrast agents of different molecular weights, gadolinium-diethylene triamine pentaacetic acid (Gd-DTPA; 0.6 kDa) and Gadomer-17 (17 kDa), in 18 spontaneous canine mammary tumors. Measurements of $F\rho$ and v_b corresponded well with literature values, and the mean $PS\rho$ measured using Gd-DTPA was a factor of 15 higher than that measured using Gadomer-17. J. Magn. Reson. Imaging 2000;12: 991–1003. © 2000 Wiley-Liss, Inc.

Index terms: breast MRI; contrast media; pharmacokinetics; dynamic MRI

IT HAS BEEN NOTED that different pathologies (eg, benign and malignant tumors) tend to exhibit different temporal patterns of contrast enhancement on dynamic contrast-enhanced MRI of the breast, and the use of this observation in the assessment of tumors has been studied extensively over the past decade (1). The distinctive shapes of the MRI contrast enhancement versus time curves observed reveal differences in the underlying physiologies of different tumor types. The curve shapes are determined in part by physiologic factors such as capillary permeability, tissue perfusion, intravascular volume, and volume of the interstitial or extracellular, extravascular space (EES) (1). Parameters related to the above physiologic factors can be measured by modeling the time course of contrast enhancement (2–10). The parameters thus derived are of great interest as indicators of tumor angiogenesis, an essential component of the growth of tumors (10–12). As such, the parameters have potential applications in diagnosis, in determining patient prognosis, in predicting which patients will respond to a particular treatment, and in evaluating treatment effectiveness (13,14).

The different approaches to the measurement of kinetic parameters from contrast-enhanced MRI have recently been reviewed (15,16). When tracer (ie, contrast agent) transport is neither flow limited nor diffusion limited, as is likely the case for small molecular weight contrast agents in breast tumor tissue, the transfer constant or exchange parameter (K^{trans}) measured using these models depends on both the tissue blood flow ($F\rho$) and the capillary permeability-surface area product ($PS\rho$). The functional significance of the transfer constant is therefore difficult to interpret, being affected by changes in both $F\rho$ and $PS\rho$. Furthermore, the models assume either that the capillary transit time is negligible or that the contribution of intravascular tracer to tissue enhancement is negligible. If these assumptions are not valid, a bias is introduced into the model parameter measurements (17,18). Therefore, in this paper, we investigate the use of a more realistic tracer kinetic model, the Johnson and Wilson model (17,19), which incorporates the effects of intravascular tracer and non-negligible capillary transit time and allows simultaneous measurement of $PS\rho$ and $F\rho$.

A relatively recent development in contrast-enhanced breast MRI is the use of large molecular weight contrast agents, such as albumin/gadolinium-diethylene tri-

[1]Imaging Division, Lawson Health Research Institute, St. Joseph's Health Care, London, Ontario, Canada, N6A 4V2.

[2]Imaging Research Laboratories, The John P. Robarts Research Institute, London, Ontario, Canada, N6A 5K8.

[3]Department of Diagnostic Radiology and Nuclear Medicine, the University of Western Ontario, London Health Sciences Centre-University Campus, London, Ontario, Canada, N6A 5A5.

[4]Imaging Diagnostics Research, MRI, Schering AG, 13342 Berlin, Germany.

Contract grant sponsor: Schering AG; Contract grant sponsor: the Canadian Breast Cancer Research Initiative of the National Cancer Institute of Canada; Contract grant number: 009408.

Presented in part at the ISMRM 7th Annual Meeting, 1999.

*Address reprint requests to: T.-Y.L., Department of Radiology, St. Joseph's Health Centre, 268 Grosvenor Street, London, Ontario, Canada N6A 4V2. E-mail: tlee@lri.sjhc.london.on.ca

Received January 5, 2000; Accepted August 18, 2000.

amine pentaacetic acid (Gd-DTPA), in various animal models. The permeability of any membrane is a function of the size of aqueous pores in the membrane and the size (radius) of the solute (20). A solute whose effective radius is more closely matched to the pore size of the membrane will be a more sensitive probe of permeability differences than a solute that is much smaller than the pore size of the membrane. Most contrast-enhanced breast MRI studies have used the contrast agent Gd-DTPA (molecular weight 0.6 kDa) and agents of similar size. This contrast agent may be too small to distinguish a permeability difference between benign and malignant breast tumors, if it exists. Several recent animal studies indicate that large molecular weight contrast agents may be more effective in detecting small permeability differences than is Gd-DTPA (6,21–24). A technique for the direct measurement of PSρ would be a useful tool for examining PSρ differences between different sized contrast agents and between tumor types with the confounding effects of perfusion differences removed.

In this paper, a technique is introduced for the simultaneous measurement of three tumor vascular parameters: blood flow (Fρ), blood volume (v_b), and the capillary permeability-surface area product (PSρ), in tumors using dynamic contrast-enhanced MRI and the Johnson and Wilson model. In addition, the technique is tested in a spontaneous mammary tumor canine model using two contrast agents of very different molecular weights: Gd-DTPA (Magnevist, Berlex Canada, Lachine, PQ, Canada), an extravascular contrast agent with a molecular weight of 0.6 kDa, and Gadomer-17 (24-Gd-macrocyclic-dendrimer) (Schering AG, Berlin, Germany), an experimental blood pool contrast agent with a molecular weight of 17 kDa. Note that due to strong water binding, the size (Stoke radius) of Gd-DTPA is similar to that of a small protein with a molecular weight of 1–2 kDa, while the size of Gadomer-17 is similar to a protein with a molecular weight of 30–35 kDa.

THEORY

Tracer Kinetic Model

The tracer kinetic model that we chose to use in this study is a relatively simple distributed parameter model first proposed by Johnson and Wilson in 1966 (19). In this model, the space in which tracer is distributed is divided into two concentric cylinders, with tracer exchanging between them (Fig. 1). The inner cylinder is the plasma space, and contrast agent concentration varies both with time and with distance along this cylinder. The outer cylinder, the interstitial space (EES), is a well-mixed compartment, and concentration in this cylinder varies with time only. A closed-form time domain solution to this model, which, in this paper, we will refer to as the adiabatic approximation to the Johnson and Wilson model (aaJW model), has recently been developed in our laboratory, using the adiabatic approximation suggested by Lassen and Perl (17,25). There are several advantages to the use of this model. First, the relative mathematical simplicity of this solution facilitates its practical application. Second, since it models a gradient in tracer concentration along the capillary bed, it represents tracer transit in breast tissue more realistically than the frequently used compartmental models. Third, since it models the first pass transit of contrast agent, very short experimental durations (<3 minutes) may be used. Finally, it allows simultaneous measurement of Fρ, PSρ, and v_b.

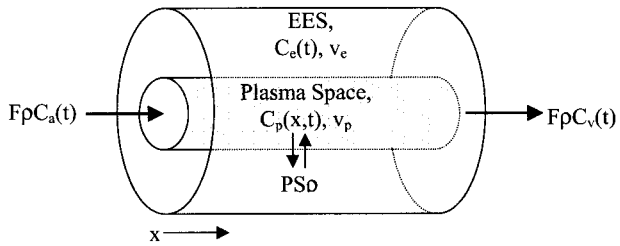

Figure 1. The Johnson and Wilson model. $C_a(t)$ and $C_v(t)$ (mM) are the concentrations of contrast agent in arterial and venous whole blood, respectively. $C_e(t)$ (mM) and $C_p(x,t)$ (mM) are the concentrations of contrast agent in the extracellular extravascular space (EES) and plasma space, respectively. $F\rho$ (min^{-1}) is the blood flow per unit volume of tissue, PSρ (min^{-1}) is the capillary permeability surface area product per unit volume of tissue, v_e is the fractional volume of the EES, and v_p is the fractional volume of the plasma space.

Assuming linearity of measurement response and that blood flow remains constant over the measurement period, the concentration of contrast agent in a volume of breast tissue ($C_t(t)$, [mM]), also called the tissue residue function (TRF), is given by linear superposition:

$$C_t(t) = F\rho C_a(t) \otimes R(t) \qquad (1)$$

where F (ml/min/g) is the blood flow, ρ (g/ml) is the tissue density, $C_a(t)$ (mM) is the concentration of contrast agent in arterial blood, or the arterial input function (AIF), and ⊗ denotes the convolution operation. Note that in this paper, we will include ρ explicitly in the parameter names to indicate that the tracer kinetic parameters are measured per volume of tissue, in contrast to more traditional measurement techniques such as autoradiography, which give parameter values per mass of tissue (15,16). $R(t)$ denotes the impulse residue function (IRF). The IRF is the TRF that would be observed if a unit amount of contrast agent were introduced instantaneously into the tissue vasculature at the site of interest. In essence it removes the confounding effects of dispersion of contrast agent in the air and recirculation from the observed TRF. As a result, the examination of impulse residue functions provides a simple way of comparing tracer kinetic models.

The impulse residue function for the aaJW model is (17):

$$\begin{aligned} R(t) &= 1 && 0 \le t < T_c \\ R(t) &= E e^{-EF\rho/v_e(t-T_c)} && t \ge T_c \end{aligned} \qquad (2)$$

where T_c (seconds) is the mean capillary transit time (average time taken for blood to traverse the capillary bed), v_e (unitless) is the fractional volume of the extra-

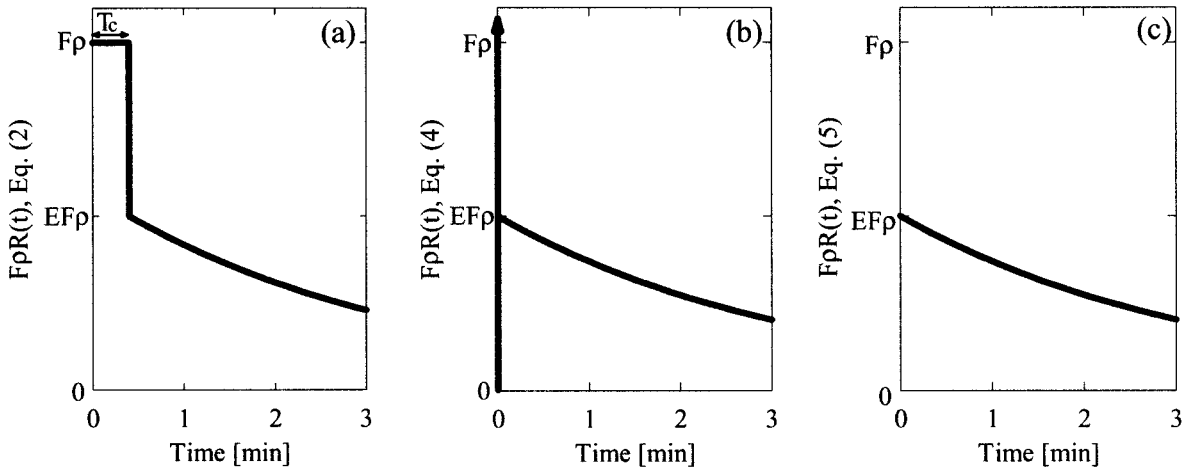

Figure 2. A comparison between the flow-scaled IRFs [= $F\rho\ R(t)$] of three tracer kinetic models. **a:** The aaJW model (Eq. [2]). **b:** The aaJW model under the condition that T_c is negligible relative to the interval at which the TRF is sampled (Eq. [4]). **c:** The aaJW model under the condition that intravascular tracer is negligible (Eq. [5]). For the full aaJW model, v_b is given by the area under the plateau (vascular) phase of the flow-scaled IRF: $v_b = F\rho T_c/60$.

cellular extravascular space (EES), and E is the extraction ratio. The extraction ratio is the fraction of tracer that diffuses unidirectionally from plasma into tissue during a single transit through the capillary bed. It is related to Fρ and to the PSρ (ml/min/g) according to (16,26,27):

$$E = 1 - e^{-PS\rho/F\rho(1 - r\mathrm{Hct})} \quad (3)$$

The factor (1 − rHct), where Hct is the large vessel hematocrit, and r is the ratio of small to large vessel hematocrit (r ≈ 0.7) (28), converts whole blood quantities such as whole blood flow (Fρ), fractional blood volume (v_b) (unitless), and arterial concentration of tracer in whole blood [$C_a(t)$] into the corresponding blood plasma quantities: plasma flow (= Fρ(1 − rHct)), fractional plasma volume [$v_p = v_b(1 - r\mathrm{Hct})$], and arterial concentration of tracer in plasma [$C_p(t) = C_a(t)/(1 - r\mathrm{Hct})$]. For a typical central venous hematocrit of 0.4, the factor (1 − rHct) is 0.72. The aaJW model therefore has five free parameters: $F\rho$, E, T_c, v_e, and the time shift between the AIF and TRF, t_0. The fractional whole blood volume, v_b, can be calculated from Fρ and T_c through $v_b = F\rho T_c/60$, and PSρ can be determined from $F\rho$ and E using Eq. [3] (17). Note that the blood volume thus calculated represents the volume of blood that is flowing in the tumor microvasculature at the time of measurement. This measure of vascularity is therefore distinct from the microvessel density vascularity metric determined from staining of tissue specimens.

If the mean capillary transit time, T_c, is negligible relative to the time interval at which the AIF and TRF are sampled, then the aaJW model reduces to (17):

$$C_t(t) = EF\rho C_a(t) \otimes e^{-EF\rho/v_e t} + v_b C_a(t) \quad (4)$$

This is the same as the operational equation used in several recent contrast-enhanced breast MRI studies (23.24). The model can be further simplified if the contribution of tracer in the intravascular space to $C_t(t)$ can be considered negligible ($v_b = 0$):

$$C_t(t) = EF\rho C_a(t) \otimes e^{-EF\rho/v_e t} \quad (5)$$

This model is identical to the consensus model described by Tofts and coworkers (16):

$$C_t(t) = \frac{K^{trans}}{(1 - r\mathrm{Hct})} C_a(t) \otimes e^{-K^{trans}/(1 - r\mathrm{Hct})/v_e t} \quad (6)$$

except that it formally defines K^{trans} [min^{-1}], the forward transfer constant between blood plasma and the EES, as EFρ(1 − rHct). Figure 2 compares the IRFs for these three models: the complete aaJW model (Eq. [2] and Fig. 2a), the case where the capillary transit time is negligible (Eq. [4] and Fig. 2b), and the case where intravascular tracer is negligible (Eqs. [5] and [6], and Fig. 2c).

If either of the assumptions of negligible intravascular tracer or negligible mean capillary transit time is violated, a bias will be introduced into the tracer kinetic parameter measurements made using either Eq. [4] or Eq. [5] (17). Since some tumors are known to be vascular, signal arising from the intravascular space may not be negligible. This will be particularly true when large molecular weight contrast agents (that are principally confined to the intravascular space) are used, since in this case there will be a smaller relative concentration of contrast agent in the interstitial space. Since the capillary transit time in breast tumors has not been determined, it is unknown whether it is reasonable to assume that T_c is negligible. However, using the mean F of 0.3 ml/min/g measured by Wilson et al (20) in human breast tumors, and a 10% blood volume, we estimate that T_c in breast tumors is approximately 20 seconds. This is not negligible relative to the temporal sampling intervals used in most tracer kinetic modeling studies, and relative to the temporal sampling recommenda-

tions made recently for Eq. [4] (30). Since it is likely that the assumptions of negligible intravascular tracer and negligible capillary transit time are violated for MR contrast agents in breast tumor tissue, the complete aaJW model (Eqs. [1] and [2]) was chosen to fit to the dynamic contrast-enhanced MR data in this study.

Another advantage to the use of the aaJW model is that it enables simultaneous measurement of Fρ and PSρ, whereas in the models of Eqs. [4], [5], and [6], these two parameters are coupled in the term EFρ or K^{trans} [= EFρ (1 − rHct)]. If the plasma blood flow is much greater than the PSρ, (min^{-1}), then transport is PS limited, and K^{trans} is equal to PSρ. On the other hand, if PSρ and plasma blood flow are of the same magnitude, then, as discussed above, K^{trans} is equal to the product of the extraction ratio (E) and plasma blood flow (Fρ(1 − rHct)). If transport is not PS limited (ie, if E > 0.2), then measurements of K^{trans} will significantly underestimate PSρ, and the reliable separation of permeability differences will be affected. Daldrup et al (31) measured a mean F of 0.24 ± 0.07 ml/min/g using microspheres and a mean E of 0.20 ± 0.11 in a rat mammary carcinoma model. This would imply that K^{trans} is a good measure of PSρ. On the other hand, Wilson et al (29) measured blood flows between 0.1 and 0.8 ml/min/g (mean 0.30 ± 0.17 ml/min/g) in human breast cancers, and measurements of K^{trans} made with Gd-DTPA have ranged between 0.1 and 2.0 ml/min/g (2,5,23,31–33). The fact that measurements of K^{trans} and F are of the same magnitude points to a large value of E (and PSρ) in at least some breast tumors, and measurements of K^{trans} may therefore mask some permeability differences. It is therefore desirable to use a model in which both Fρ and PSρ can be measured simultaneously.

Calibration of MR Image Intensities

A saturation-prepared turbo fast low-angle short (FLASH; SPTF) sequence, in which magnetization is initially saturated by a nonselective 90° radiofrequency (RF) pulse followed after a delay time TI by a turbo-FLASH acquisition, was chosen for the dynamic MR imaging (34). RF spoiling was used, as well as constant gradient spoiling on the phase-encode and readout axes (35). This sequence was chosen to enable measurement of an arterial input function (AIF). Fritz-Hansen et al (36) demonstrated that the AIF could be accurately measured using an inversion-prepared FLASH sequence. The sequence used in this study is similar, except that a saturation preparation pulse, rather than an inversion preparation pulse, was used to make image intensity independent of heart rate and arrhythmias (37,38). The sequence was triggered by the R-wave on the electrocardiogram (ECG) so that the center of k-space was acquired at end-diastole to minimize inflow effects. The MR signal (S) generated by the SPTF sequence is (36,39):

$$S = K\left((1 - e^{-TI/T_1})a^{n-1} + (1 - E_r)\frac{1 - a^{n-1}}{1 - a}\right),$$
$$E_r = e^{-TR/T_1},\ a = E_r\cos(\alpha) \quad (7)$$

where α is the tip angle of the excitation pulses in the turbo-FLASH sequence, TR is the time between α-pulses, TI is the time from the saturation pulse to the first α-pulse in the turbo-FLASH sequence, and n is the number of phase-encode lines acquired before acquisition of the center of k-space. K is a scaling factor, which is dependent on proton density, T_2^*, receiver gain and α, and is assumed constant as a function of time. The addition of a concentration of contrast agent ([CA]) to a volume of tissue changes the bulk T_1 relaxation time of the tissue according to:

$$\Delta R_1 = \frac{1}{T_1} - \frac{1}{T_{10}} = r_1[CA] \quad (8)$$

where ΔR_1 is the change in T_1 relaxation rate, T_{10} is the precontrast T_1 of the tissue, and r_1 is the T_1 relaxivity of the contrast agent in the tissue. In principle, if T_{10} is measured and if TR, α, TI, and n are known, then, using Eq. [7], measurements of precontrast and postcontrast image intensity can be used to determine postcontrast T_1 (40). Measurements of T_1 can then be converted into ΔR_1, which in turn is proportional to contrast agent concentration (Eq. [8]).

MATERIALS AND METHODS

Animal Protocol

Twenty-five pet dogs with palpable spontaneous mammary tumors were recruited into the study over a period of 16 months. The dogs were between 5 and 15 years old [10 ± 3 (SD) years] and weighed between 2 and 40 kg [21 ± 14 (SD) kg]. Informed consent was obtained from the dog owners. The animals were treated in accordance with the guidelines set out by the University of Western Ontario University Council on Animal Care Animal Use Subcommittee, and the facility is accredited by the College of Veterinarians of Ontario. The dogs were anesthetized with 1.5%–2.0% isoflurane and were given intravenous injections of benadryl (1.0–2.0 mg/kg) and dexamethosone (0.4 mg/kg) 15 minutes prior to the first bolus injection. Each dog was wrapped in a water heating pad to maintain body temperature at 37°C throughout MR imaging.

MRI

All imaging was done on a 1.5-T Siemens Vision MR scanner (Siemens, Erlangen, Germany). The dogs were placed supine in either a circularly polarized (CP) extremity, CP head, or large CP flex RF coil, depending on the size of the dog. The saturation prepared turbo-FLASH (SPTF) sequence was employed for both the precontrast T_1 measurement and the dynamic imaging. T_{10} was measured by repeating the SPTF sequence for eight different times (TI) between the saturation pulse and the first α-pulse and fitting the resulting saturation-recovery data using Eq. [7]. The sequence parameters for the SPTF sequence were as follows: TR/TE 3.7/1.2 msec, α 15°, slice thickness 8 mm, and field of view (FOV) 370 mm. For the T_1^O measurement, the TI times used were 2500, 2000, 1500, 1000, 500, 250, 100, and

9 msec, and four images were averaged for each TI. Either a 64 × 128 or a 96 × 128 matrix size (phase × frequency, rectangular FOV) was used, depending on the size of the dog. For the dynamic imaging, a 128 × 128 matrix size and a TI of 9 msec were used, giving an effective TI (ie, time from the saturation pulse to acquisition of the center of k-space) of 248 msec, and a total acquisition time of 490 msec.

Phantom Experiments

Two phantoms, each consisting of 16 aqueous solutions of Gd-DTPA (Magnevist, Berlex Canada) or Gadomer-17 (Schering) in vials 30 mm in diameter were constructed. The concentrations of Gd-DTPA ranged between 0 and 4 mM, and the concentrations of Gadomer-17 ranged between 0 and 1 mM. These phantoms were used to investigate the validity of the signal equation of the SPTF pulse sequence (Eq. [7]) and the precontrast T_1 measurements.

The accuracy of the T_1 measurement technique was assessed by comparing T_1 measurements made in the phantoms using the SPTF method with T_1 measurements made using an inversion-recovery spin-echo (IR-SE) imaging sequence. The 64 × 128, 96 × 128, and 128 × 128 matrix sizes (head coil only) were investigated, and all RF coils used in the dog imaging were tested using the 64 × 128 matrix size. The IR-SE measurements were done using the transmit/receive head RF coil with the phantoms placed inside the head coil cylindrical loader shell, which is filled with doped saline. The IR-SE sequence parameters were as follows: TR/TE 4000/20 msec, slice thickness 10 mm, 128 × 128 matrix, FOV 300 mm, and TI 2000, 1500, 1000, 750, 500, 250, 100, 20 msec. A three-parameter (A, B, and T_1) equation:

$$S(\mathrm{TI}) = A(1 - Be^{-\mathrm{TI}/\mathrm{T_1}}) \qquad (9)$$

was fit to the data from the IR-SE sequence, and Eq. [7] was fit to the data from the multiple TI SPTF experiment to determine T_1, K, and α.

The signal from the SPTF sequence is known to saturate at high contrast agent concentrations (38,41). Generally, in tissue, the contrast agent concentrations are low enough so that the signal intensities are in the linear range. In the artery, however, there is a potential for signal saturation, which would result in large errors in the parameter estimates. The phantoms were therefore used to verify the conversion between change in image intensity and ΔR_1 and to determine at what [CA] saturation of the MR signal becomes problematic. The Gd-DTPA and Gadomer-17 phantom sets were imaged using the SPTF sequence with 10 acquisitions and α = 5°, 10°, 15°, 20°. A relative enhancement factor was calculated for each vial of each phantom: $(S - S_0/S_0$, where S is the image intensity of the vial, and S_0 is the image intensity in a baseline vial. In this way, tissue enhancement versus contrast agent concentration curves were simulated, with the baseline vial representing precontrast tissue. Different precontrast T_1s were simulated by taking different vials as the baseline (precontrast) vial and redefining contrast agent concentration as the difference between that of each vial and the baseline vial.

Animal Experiments

Following tumor localization, an axial slice through the tumor was selected, and T_{10} was measured. A single SPTF image slice was acquired 120 times, with the acquisition triggered to every second heartbeat, resulting in a temporal resolution of approximately 1.5 seconds and a total imaging time of approximately 3 minutes. After the acquisition of 10 baseline images, Gadomer-17 or Gd-DTPA was injected intravenously either manually over approximately 10 seconds (dogs 1–5) or automatically at a rate of 0.64 ml/sec (dogs 6–25) using an infusion/withdrawal syringe pump (Harvard Apparatus, South Natick, MA). The entire procedure, including the T_{10} measurement, was repeated for both contrast agents. Complete clearance of contrast agent between injections is not required since ΔR_1 is determined from the change in image intensity relative to a baseline value. Since at 30 minutes post contrast the intensity in arterial blood and in tumor tissue is effectively constant over the 3-minute measurement time, bolus injections of contrast agent were spaced at least 30 minutes [32–65 minutes, mean = 39 ± 8 (SD) minutes] apart.

In all but three dogs, Gadomer-17 was injected first since it was expected that, compared with Gd-DTPA, less of the contrast agent would accumulate in the tissue and since the baseline was expected to be more flat for subsequent injections. As a check for systematic errors arising from the injection order, the injection order was reversed for three dogs. The doses of Gadomer-17 and Gd-DTPA injected were 0.0085/0.015 and 0.025/0.045 mmol/kg, respectively. (Three dogs received the high doses.) The dose of Gadomer-17 injected was three times lower than the dose of Gd-DTPA injected to account for the difference in relaxivities of the two contrast agents, so that approximately the same peak ΔR_1 in blood would be obtained for the two contrast agents. The doses of both contrast agents were low relative to the recommended clinical doses; this was done in order to avoid saturation of the arterial input function. For each dog, all injections were standardized to the same volume, 0.2 ml/kg, with a minimum volume of 2 ml, by diluting the contrast agent with saline.

Image Analysis

Image intensity versus time curves were constructed for two regions of interest (ROIs), one encompassing the whole tumor and the other within the aorta. Regions within the tumor that did not enhance, as determined from subtraction of an image acquired at 3 minutes post contrast from a baseline image, were excluded. A time was assigned to each data point using the R-R and trigger intervals. The precontrast T_1 (T_{10}) of the tumor ROI was determined for each injection by fitting Eq. [7] to the saturation recovery data. The precontrast T_1 of arterial blood could not be measured due to difficulties in triggering the SPTF sequence for long TI times. A T_{10} of 1260 msec was therefore assumed for arterial blood

for the injection of the first contrast agent (42), and T_{10} for subsequent injections was inferred from the change in baseline signal intensity using Eq. [7]. The intersubject variability of T_{10} of arterial blood is small, and so the uncertainty introduced into the parameter measurements by this assumption will also be small. Tadamura et al (42) report a mean arterial blood T_{10} of 1260 ± 80 (SD) msec in six individuals, and Noseworthy et al (43) report a mean arterial blood T_{10} of 1205 ± 58 (SE) msec in seven individuals.

The MR image intensity following contrast agent administration was converted into ΔR_1 using the precontrast T_1, the baseline (precontrast) image intensity, and the signal equation for the SPTF sequence (Eq. [7]). This step corrects for the nonlinearity of the SPTF signal equation with ΔR_1. Since ΔR_1 is proportional to contrast agent concentration (Eq. [8]), the ΔR_1 curves can be used for the AIF and TRF assuming that r_1 is the same in plasma and tissue. This assumption is supported by the finding of Donahue et al (44) that the r_1 of Gd-DTPA is the same in saline, plasma, and cartilage (a model of interstitium) at 8.45 T and room temperature. In order to correct for the difference between the central venous and tissue hematocrit, the measured arterial input function was multiplied by (1 − rHct)/(1 − Hct).

Curve Fitting

The aaJW model was fit to the ΔR_1 versus time curves using the quasi-Newton bounded minimization algorithm E04JAF from the NAG FORTRAN library (Downers Grove, IL). Due to the presence of local minima, the minimization algorithm is extremely sensitive to initial guess if all five parameters ($F\rho$, E, T_c, v_e, and time shift) are fit simultaneously. The algorithm was stabilized by linearly stepping through values of T_c from 1 to 60 seconds, thereby systematically trying many starting points. For each T_c, the optimal $F\rho$, E, v_e, and time shift were found. The final solution was taken as the solution that minimized the sum of squared differences between the data and the fit. All model parameters were constrained to be non-negative, as negative values are nonphysiologic. E was further constrained to be less than 1.0, and v_e was constrained to be greater than 0.1. An estimate of the uncertainty (SD) arising from noise in the TRF in each of the parameter estimates was determined from the aaJW model's covariance matrix calculated at the optimum parameter values, with the variance in the TRF estimated from the data (45). $PS\rho$ was calculated from $F\rho$, E, and Hct using Eq. [3], and v_b was determined from the product of $F\rho$ and $T_c/60$ (17).

Statistics

Statistical analysis was performed using the SigmaPlot and SigmaStat statistical software package (SPSS, Chicago IL). Standard descriptive statistics parameters, such as mean, median, and SD were found. The existence of linear correlations between parameters was evaluated using the Pearson product moment correlation. A paired t-test was used to compare the means of parameter measurements made with the two contrast agents. Statistical significance was declared at $P < 0.05$.

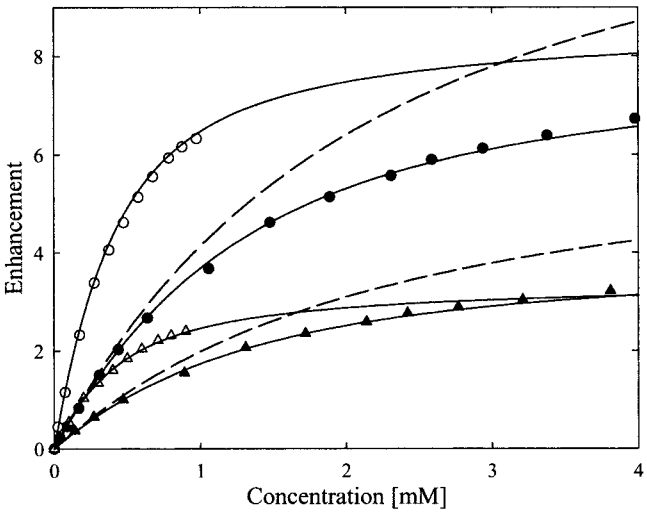

Figure 3. Enhancement versus contrast agent concentration curves measured in aqueous solution for Gadomer-17 with T_{10} = 1385 msec (open circles) and T_{10} = 572 msec (open triangles) and for Gd-DTPA with T_{10} = 1308 msec (filled circles) and T_{10} = 661 msec (filled triangles). The corresponding curves calculated from the SPTF signal equation with the prescribed tip angle divided by 1.5 are also plotted (solid lines). For comparison, the SPTF signal equation calculated using the prescribed tip angle (α = 15°) is plotted using a dashed line for the Gd-DTPA data only.

RESULTS

Phantom Experiments

The mean error of the SPTF method for T_1 measurement in eight of the Gd-DTPA phantoms having T_1s ranging between 185 and 1300 msec was under 5% for all matrix size and RF coil combinations tested, and the maximum bias observed in any phantom was −8%. The T_1 relaxivities of Gd-DTPA and Gadomer-17 measured in saline at 20°C were 0.00461 mM^{-1} ms^{-1} and 0.0136 mM^{-1} ms^{-1}, respectively.

The phantom experiments showed that the SPTF signal saturates more than what is predicted by the theoretical signal equation (Eq. [7]). This is because, while the signal equation assumes a rectangular slice profile, in reality α will vary across the slice. This problem is encountered whenever signal equations are used to extract T_1 values from 2D images, and the solution is either to incorporate an integration across slice profile into the signal equation or to construct a calibration curve (40,46–48). In this study, the latter approach was taken, and it was determined empirically that a good match between theory and data can be obtained, independent of α and T_{10}, if the nominal α is divided by a factor of 1.5. Although it is not strictly correct to do so, this effective α can be thought of as a weighted average of the true α across the slice profile. A comparison between the phantom data and the corrected signal equation is shown in Fig. 3. Due to its higher r_1, the Gadomer-17 signal saturates at lower [CA] than does the Gd-DTPA signal. The signal equation can be used to correct for some degree of signal nonlinearity with concentration, but because of signal saturation at high [CA], the maximum anticipated contrast agent concen-

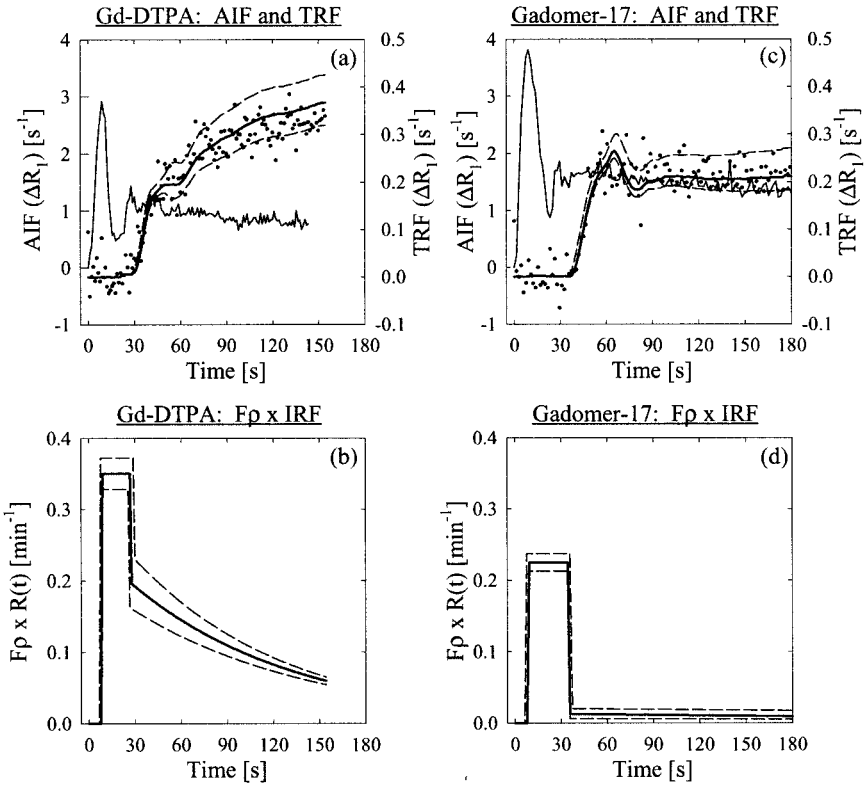

Figure 4. Representative AIF and TRF acquired following contrast agent injection in the same dog, together with the corresponding flow-scaled IRFs estimated with Eqs. [1] and [2]. **a:** AIF and TRF after Gd-DTPA injection. **b:** Flow-scaled IRF for the Gd-DTPA injection. **c:** AIF and TRF after Gadomer-17 injection. **d:** Flow-scaled IRF for the Gadomer-17 injection. In a and c) AIFs are indicated by a thin line, the TRF data are represented as filled circles, with a thick black line showing the best fit through the data, and the thin lines show the ± SD confidence interval. In b and d, the flow-scaled IRF is the solid line, and the dashed lines show the ± SD confidence interval.

trations should be kept below approximately 1 mM for Gd-DTPA and 0.3 mM for Gadomer-17. In humans, the maximum concentration in the AIF after a short bolus injection of 0.1 mmol/kg Gd-DTPA is 4 mM (36). Significant saturation of the AIF will therefore be avoided by reducing the dose of Gd-DTPA injected to 0.025 mmol/kg,

Animal Experiments

Results were obtained for 18 of the 25 dogs studied. Six dogs were excluded from the study since artery sizes at the level of the tumor were too small to permit an AIF measurement, and a seventh dog was excluded since ECG gating of data acquisition could not be achieved. In two tumors, no enhancement was observed, and so tracer kinetic analysis was not done. Tumor ROIs ranged in size from 5 to 244 pixels (27–1340 mm^2), with a mean size of 74 ± 73 (SD) pixels. The mean SNR in the TRF was 11 ± 7 (SD) and 12 ± 8 (SD) for Gadomer-17 and Gd-DTPA, respectively, and the mean SNR in the TRF per pixel was 0.4 ± 0.4 and 0.4 ± 0.3 for Gadomer-17 and Gd-DTPA, respectively. The mean sampling interval was 1.4 ± 0.2 (SD) seconds.

In all cases, the aaJW model (Eq. [2]) fit the data very well. The mean chi-square of the fits was 174 ± 84 (SD, range 75–365) for Gadomer-17 and 131 ± 59 (SD, range 75–333) for Gd-DTPA. Typical results for one dog are shown in Fig. 4. In Fig. 4a and c, the measured AIF is superimposed on a graph of the measured TRF and the fit for both the Gd-DTPA (Fig. 4a) and Gadomer-17 (Fig. 4c) injections. The different shapes of the TRFs measured with the two contrast agents illustrate the effect of the different sizes of the two contrast agents. The Gadomer-17 TRF has a much more prominent vascular phase (indicated by the peak in the early part of the TRF) than does the Gd-DTPA TRF. Also, in the Gd-DTPA TRF, the contrast agent is still accumulating in the tissue at the end of 3 minutes, while with Gadomer-17, the contrast agent concentration has reached a plateau. The corresponding flow-scaled IRFs are shown in Fig. 4 b and d. It is clearly seen that much less contrast agent is left in the tissue after the vascular phase (rectangular part of IRF) for Gadomer-17 than for Gd-DTPA, and therefore that E for Gadomer-17 is considerably smaller than E for Gd-DTPA.

The tracer kinetic parameter measurements made with Gadomer-17 were compared with those made with Gd-DTPA (Fig. 5). Note that the error bars in this figure show the standard deviation in the individual parameter measurements determined from the COV calculated at the fit. There was a strong correlation (r = 0.907) between $F\rho$ measured with Gd-DTPA and Fρ measured with Gadomer-17. Similarly, v_b measurements made with the two contrast agents were also strongly correlated (r = 0.882). In addition, systematically higher values of $F\rho$ and v_b were measured with Gd-DTPA compared with Gadomer-17: a linear regression through the $F\rho$ and v_b data gave slopes of 1.3 and 2.0, respectively. On the other hand, the measurements of PSρ and E made with Gd-DTPA did not correlate significantly with those made using Gadomer-17. In this case, the correlation coefficients were 0.486 for PSρ and 0.157 for E.

Table 1 lists the mean and standard deviation of the tracer kinetic parameter estimates made using Gd-DTPA and Gadomer-17. Values of v_e measured using

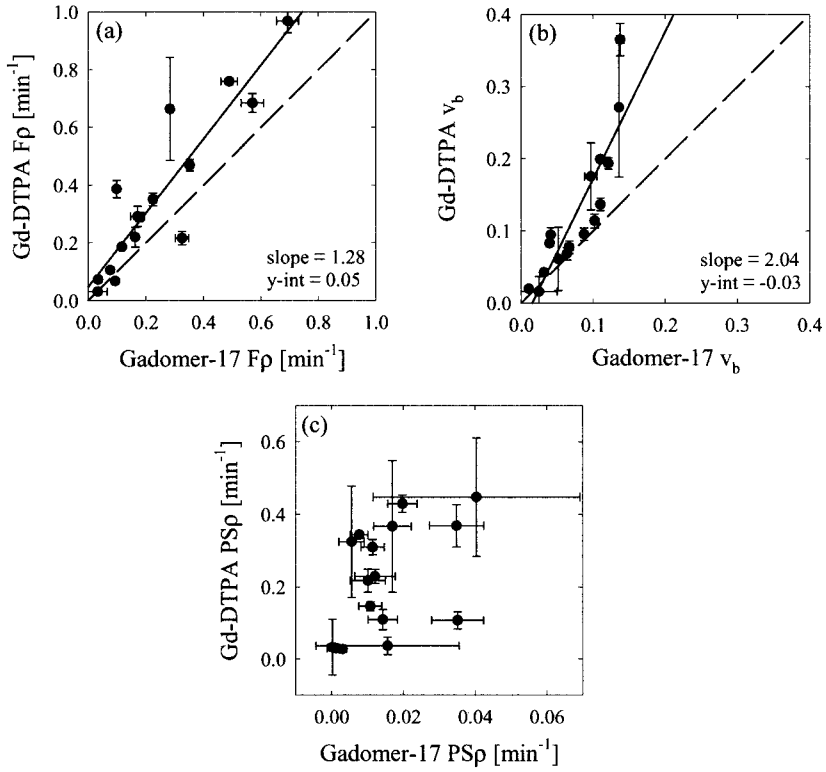

Figure 5. Comparison between Gadomer-17 and Gd-DTPA measurements of (**a**) Fρ, (**b**) v_b, and (**c**) of PSρ. Error bars are the SD of the measurement estimated from the covariance matrix. The solid line indicates a linear regression through the data, and the dashed line is the line of identity.

Gadomer-17 are not reported since for this contrast agent the uncertainty in the v_e measurement is very large. For large molecular weight contrast agents (small *E*), the aaJW model has minimal sensitivity to v_e, since in this case the concentration of contrast agent in the EES will be relatively small and will therefore have only a minimal effect on the shape of the TRF.

Results from the two tumors that did not enhance were not included in the calculations. The mean T_c for Gd-DTPA was not significantly different from the mean T_c for Gadomer-17. There was, however, a significant difference between the means of all other parameters measured using the two contrast agents. In particular, the overall mean PSρ measurement was 15 times higher for Gd-DTPA compared with Gadomer-17, indicating a strong dependence of PSρ on the molecular weight of the contrast agent.

DISCUSSION

Tumor Model

Since Gadomer-17 has not yet been approved for use in humans, it was necessary to use an animal model. The spontaneous canine mammary tumor model in pet dogs was chosen as the closest available model of human breast disease. This tumor model is ideal for investigating a diagnostic technique since there is a high prevalence of mammary tumors in dogs and since the animals develop a wide spectrum of mammary pathologies, encompassing both benign and malignant disease. Since human and canine mammary tumors share many characteristics, including species-adjusted age of onset, morphologic appearance of cells, antigenic phenotype, endocrine properties, and general course of the disease, the canine spontaneous mammary tumor model is considered to be overall a good model of human breast cancer (49–51).

Table 1
Mean (±SD) Parameter Measurements Made with Gd-DTPA and Gadomer-17

Parameter	Gd-DTPA	Gadomer-17
$F\rho$ (min^{-1})	0.36 ± 0.28	0.24 ± 0.20
v_b	0.13 ± 0.09	0.077 ± 0.041
$PS\rho$ (min^{-1})	0.22 ± 0.15	0.015 ± 0.012
v_e	0.50 ± 0.30	—
T_c (s)	24 ± 9	25 ± 15
E	0.56 ± 0.15	0.10 ± 0.10
$EF\rho(1 - rHct)$ (min^{-1})	0.15 ± 0.10	0.014 ± 0.011

Features of the Study

In order to apply a tracer kinetic model to make quantitative measurements of blood flow (Fρ), blood volume (v_b), and capillary permeability (PSρ), several factors must be considered (52). Measurements of precontrast T_1 (needed to convert MR image intensity into contrast agent concentration) and of the AIF should be made. In addition, the AIF and TRF should be sampled sufficiently frequently to ensure accurate measurements of the tracer kinetic parameters (30). The exact temporal sampling requirements depend on the tracer kinetic model. For the aaJW model (Eq. [2]) and typical vascular parameters found in breast tumor tissue, we have previously determined that if the SNR in the TRF is greater than 10, the AIF and TRF should be sampled every 1.5 seconds (53). In this study, these requirements have been fulfilled by measuring tumor T_{10} and each individual AIF, and by sampling approximately every 1.5 seconds.

The tracer kinetic model used in these experiments, the aaJW model, is a more realistic model of MR contrast agent transport in breast tissue than the models that have previously been used to interpret contrast-enhanced breast MRI data (Eqs. [4–6]). The model is appropriate for the study of small molecular weight contrast agents such as Gd-DTPA in breast tumor tissue, for which transport is neither flow nor PS limited, as it explicitly models the changing concentration of contrast agent along the vascular bed, and a finite capillary transit time. The main advantage to this model is that both Fρ and PSρ can be measured simultaneously, while with other models they are coupled in the term $K^{\text{trans}} = EF\rho(1 - \text{rHct})$. In addition, only a short experimental length is required. Furthermore, since the model recognizes a non-negligible mean capillary transit time, justified by our finding that $T_c \sim 25$ seconds, all parameters measured by the model are closer to the truth (more accurate) than those measured using the simpler models described by Eqs. [4–6]. On the other hand, since more parameters are modeled, it is likely that there is a reduction in the precision with which each parameter can be measured, and the high temporal sampling rate required may limit the use of this model.

Limitations of the Study

Care was taken to design the study in order to make accurate measurements of the vascular parameters. Nevertheless, a few limitations of the study methodology remain and should be recognized. First, because of the low spatial resolution ($3 \times 3 \times 8$ mm) and the ROI analysis used, our results are vulnerable to partial volume errors. Tumors are known to be spatially heterogeneous, and in this study some degree of heterogeneous enhancement was observed in all cases (54,55). Ideally, Fρ, v_b, and PSρ should be determined on a pixel-by-pixel basis; however, this requires a higher contrast-to-noise level than we were able to achieve, given the necessarily low doses of contrast agent used.

Second, the precontrast T_1 of arterial blood should be measured, rather than assumed. Since, for a T_1-weighted pulse sequence, enhancement is approximately proportional to the product of T_{10}, r_1, and contrast agent concentration (56), an error in the precontrast T_1 of arterial blood would result in a scaling error between the AIF and the TRF. This would manifest as an error in the parameter measurements. From Eq. [1] it can be seen that if the assumed T_{10} of arterial blood was too high and $C_a(t)$ therefore underestimated, Fρ would be overestimated. As a result, v_b, v_e and PSρ would also be overestimated (Eqs. [2] and [3]), while estimates of the parameters that describe the shape of the IRF, E and T_c, would be unaffected. These errors would be consistent for both contrast agents studied.

Third, another fundamental assumption to this work is that the relaxivity of the two contrast agents are the same in plasma as in tumor tissue. Following a similar argument to the above, it can be demonstrated that a discrepancy between the relaxivities in the two tissues would result in a bias in the measurement of Fρ, v_b, v_e, and PSρ. If the magnitude of the discrepancy were different for Gd-DTPA and Gadomer-17, then the magnitude of the bias would differ between Gd-DTPA and Gadomer-17. On the other hand, any such bias would be consistent over all dogs studied. Fourth, it is the nature of tracer kinetic modeling that many assumptions about the tissue system are made, and these assumptions may affect the accuracy of the parameter measurements. In practice, a compromise must be struck between the realism of the model (number of processes modeled) and the precision of the measured parameters, given the quality of the data (temporal sampling and SNR). For example, the aaJW model used assumes that the EES is a well-mixed compartment. While this assumption is somewhat justified by the random arrangement of the tumor microvessels (55), it may not hold completely. More sophisticated models do exist in which variations in concentration within the EES are accounted for (57); however, these models are too mathematically complex for the quality of the data acquired in these experiments to make their use practical.

Another limitation to this technique is suggested by the systematically higher measurement of Fρ and v_b made using Gd-DTPA relative to those made using Gadomer-17. The same trend existed regardless of which contrast agent was injected first. While a slightly higher measurement of Fρ made using Gd-DTPA arising from insufficient temporal sampling and noise in the TRF has been predicted by computer simulations, no such trend was predicted for v_b (53,58). Interestingly, the phenomenon of smaller contrast agents measuring higher blood volumes has been observed by others (23,24). These groups suggest that the higher blood volume measurement is due to the contrast agent, which extravasates at early times, being misinterpreted by the tracer kinetic model as intravascular contrast agent. The aaJW model, however, explicitly models the extravasation of contrast agent at early times. There are a number of possible explanations for the discrepancy we have observed.

While it has been shown that neither random noise in the TRF nor insufficient temporal sampling result in a bias in the v_b measurements with molecular weight (16), bias in this parameter could have been introduced by physiologic noise or noise in the AIF. As discussed earlier, a difference in the relative scaling of the AIF and TRF if the r_1 of blood is not equal to that of tumor tissue would also result in a bias. Alternatively, the discrepancy could indicate the existence of other processes not modeled by the aaJW model. Finally, the systematic bias observed could be due to a breakdown of the assumption of fast proton exchange that was made in order to relate the change in T_1 relaxation rate to concentration of contrast agent in Eq. [8] (59). Proton exchange rates in mammary tumors, in which elevated capillary permeability has been demonstrated, are unknown. If proton exchange between the intravascular space and the EES is slow or intermediate, intravascular contrast agent will be effectively hidden from the majority of water protons that reside in the cellular and interstitial tissue compartments. Under these condi-

Table 2
Comparison Between Mean Measurements of Vascular Parameters in Breast Tumors Reported in the Literature*

Reference	Tumor model	CA	K^{trans} (min^{-1})	v_b	v_e	K^{trans}/v_e (min^{-1})
Current study	Canine	Gd	0.15	0.13	0.5	0.31
Tofts et al (2)	Human	Gd	0.1–1.2[a]	—	0.3–0.8[a]	—
Su et al (24)	Rat (ENU)	Gd	—	0.04–0.10[b]	—	0.13–0.28[b]
den Boer et al (5)	Human	Gd	0.90–2.04[b]	0.24–0.36[b,c]	0.45–0.47[b]	—
Hulka et al (33)	Human	Gd	0.21–0.45[b]	—	—	—
Mussurakis et al (32)	Human	Gd	0.24–0.59	—	—	—
Daldrup et al (31)	Rat (R3230)	Gd	0.04	0.11[c]	—	0.216
Daldrup et al (23)	Rat (ENU)	Gd	0.13–0.13[b]	0.08–0.16[b,c]	—	—
Current study	Canine	G-17	0.014	0.08	—	0.04[d]
Su et al (24)	Rat (ENU)	G-17	—	0.03–0.07	—	0.07–0.11

*Parameter values that were reported for tissue mass have been converted into parameter values in a tissue volume using $\rho = 1.0$ g/ml. CA = contrast agent, Gd = Gd-DTPA, G-17 = Gadomer-17.
[a]Range of individual measurements in cancers.
[b]Range of means measured in different pathologies (eg, benign and malignant).
[c]v_p was converted into v_b according to $v_b = v_p/(1 - rHct)$, $(1 - rHct) = 0.72$.
[d]v_e was determined using Gd-DTPA.

tions, if fast proton exchange is assumed, blood flow and blood volume would be underestimated, and the degree of parameter inaccuracy would be dependent on the molecular size of the contrast agent (59,60).

Comparison of Results With Literature Values

The mean values of the tracer kinetic parameters measured in this study are comparable to those reported for breast tumors in the literature. Overall mean Fρ of 0.36 ± 0.28 min^{-1} and 0.24 ± 0.20 min^{-1} were measured using Gd-DTPA and Gadomer-17, respectively. Assuming that $\rho \sim 1.0$ g/ml, these values of blood flow correspond well with data pooled from many studies reporting F in breast carcinomas between 0.08 and 0.80 ml/min/g (61). This measurement also corresponds well with the mean F of 0.30 ± 0.17 (SD) ml/min/g measured by Wilson et al (29) in human breast cancers using ^{15}O-labeled water and positron emission tomography, and the mean F of 0.43 ± 0.12 (SD) ml/min/g (converted from plasma flow) measured by Daldrup et al (31) in a rat mammary tumor model using fluorescent microspheres. The vascular space of tumors varies from 1% to 20% (62). This is similar to the results of this study: the mean v_b measured by Gd-DTPA was 0.13 ± 0.09, and the mean v_b measured using Gadomer-17 was 0.08 ± 0.04.

Table 2 compares MR-derived tracer kinetic parameter measurements from various studies with the equivalent parameters measured in this study. Although they are determined using different tracer kinetic models, the K^{trans} determined by other studies has the same physiologic interpretation as $EF\rho(1 - rHct)$ determined in this study and is therefore expected to be the same. A comparison of the values of K^{trans} in Table 2 shows that our measurement of $EF\rho(1 - rHct)$ is within the range of K^{trans} measured by others, although it is in the lower end of the range. The mean values of v_b and v_e found in this study also fall in the middle of the range of values determined by other studies.

Effect of Tracer Molecular Weight on PSρ and E

There was a highly significant difference between the mean PSρ measurements made with the two contrast agents. The mean overall PSρ measured using Gd-DTPA ($PS\rho = 0.22 \pm 0.15$ min^{-1}) was approximately 15 times larger than that measured using Gadomer-17 ($PS\rho = 0.015 \pm 0.012$ min^{-1}). This dependence of permeability on the molecular weight of the tracer has been observed by others using different tumor models and very large macromolecules (albumin and larger) (63). Su et al (24) found that the outflux transport rate K_{21} ($\sim EF\rho/v_e$) measured in carcinomas was approximately three times higher for Gd-DTPA (0.3 min^{-1}) compared with Gadomer-17 (0.09 min^{-1}) but about the same ($\sim$0.1 min^{-1}) for the two contrast agents in fibroadenomas in a rat mammary tumor model. Although the compound nature of K_{21} would be expected to mask the permeability difference to some extent, it is interesting that we have observed a greater molecular weight dependence of the equivalent parameter (Table 2). This difference may either be due to the different tracer kinetic models used (ie, the importance of non-negligible T_c) (17), or to the different tumor models used.

The mean extraction fraction measured for Gd-DTPA in canine mammary tumor was 0.56 ± 0.15. The measurement of an E greater than 0.2 indicates that measurements of K^{trans} are not equivalent to measurements of PSρ, and that the use of the distributed parameter aaJW model is indicated. This result is similar to measured values for E of between 0.5 and 0.6 in myocardium (64). On the other hand, an extraction ratio of 0.2 was measured in a rat mammary tumor model (31). The discrepancy between our results and these rat tumor results could be due to differences between the tumor models used. According to the current study, E of Gd-DTPA in breast tumor tissue is greater than 0.2, and therefore measurements of K^{trans} in breast tumor tissue must be interpreted as $EF\rho(1 - rHct)$ rather than PSρ. For Gadomer-17, E was 0.10 ± 0.10, implying that for this contrast agent, assuming that Eqs. [4], [5], or [6]

adequately describe the tracer kinetics, measurements of K^{trans} or $EF\rho(1 - rHct)$ are equivalent to $PS\rho$.

Future Research Directions Suggested by This Study

The uncertainty in each of the parameters that was estimated from the covariance matrix (error bars in Fig. 5) represents an underestimation of the true uncertainty. Additional sources of parameter uncertainty include noise in the AIF, uncertainty in T_{10}, uncertainty in the time assignment of the data points, and temporal instability of the actual parameter values. The true precision of the parameter measurements should be determined experimentally by doing repeat experiments in each dog and analyzing the data using ANOVA of repeated measures (65).

The largest difficulty encountered in these experiments was the relatively low SNR in the TRF resulting from the necessarily low dose of contrast agent injected to avoid saturation of the AIF. It would be highly desirable to find a technique to extend the range of contrast agent concentrations over which signal intensity is linear, thereby allowing larger doses of contrast agent and improving the SNR of the TRF. Very fast T_1 mapping is one possibility (41,66). Furthermore, a significant improvement in the SNR of the TRF would allow parameters to be calculated pixel by pixel. This would allow for assessments of the degree of parameter variability within a tumor and the presence of tracer kinetic parameter "hot spots.".

Finally, several recent studies have shown improved differentiation, either between tumor grades or between tumor types, with large molecular weight compared with small molecular weight contrast agents (21–24). However there have been some inconsistencies in the reported results. On the one hand, the exchange parameter of Su et al (24) differentiated between benign and malignant tumors with small but not large molecular weight contrast agents, and did not differentiate between malignant tumor grades for any of the contrast agents studied. On the other hand, the exchange parameter of Daldrup et al (23) correlated with tumor grade with a large but not with a small molecular weight contrast agent, and Adam et al (21) could distinguish between benign and malignant tumors based on curve shape for large but not for small molecular weight contrast media. The technique we have described is particularly ideal for evaluating whether large molecular weight contrast agents are better able to distinguish between tumor types based on permeability differences as it measures $PS\rho$ rather than exchange parameters that are dependent on $PS\rho$, $F\rho$ (and v_e). In addition, the spontaneous canine mammary tumor used provides a wide variety of pathologies, and the size of the animal facilitates the measurement of the arterial input function. In future studies, the technique will be used to assess the ability of vascular parameter measurements made with different sized contrast agents to differentiate between benign and malignant canine mammary tumors (sample size constraints do not allow this assessment to be made with the current data).

CONCLUSIONS

In this study, a contrast-enhanced dynamic MRI technique for measuring $F\rho$, v_b and $PS\rho$ in spontaneous canine mammary tumors was demonstrated. Features of the technique include measurement of precontrast tumor T_1, rapid temporal sampling, measurement of the arterial input function, and use of a more realistic tracer kinetic model. Measurements of $F\rho$, v_b, and $PS\rho$ made with two different sized contrast agents (Gd-DTPA and Gadomer-17) in spontaneous canine mammary tumors were compared. E and $PS\rho$ were found to be highly dependent on the molecular weight of the contrast agent. Potential applications of measurements of $F\rho$, $PS\rho$, and v_b include the diagnosis of breast disease, the evaluation of patient prognosis, basic studies of the tumor vasculature, and the assessment of tumor response to treatment.

ACKNOWLEDGMENTS

We are grateful to Eric Jensen for his technical assistance, to Dr. Carolyn Kerr for carrying out the anesthesia, and to Dr. Gary Bouck for performing the surgeries. Thames Valley Veterinary Services, in particular Jackie Taylor and Cathy Cavanagh, provided additional animal care. We also thank the referring veterinarians and owners of the volunteer pets. We are indebted to Dr. Raoul Pereira, Dr. Charles McKenzie, and Dr. Frank Prato for their many valuable suggestions involving the MR protocol. Image analysis was performed using the Xstatpak program developed by J. Davis. Contrast agents were provided by Schering AG.

REFERENCES

1. Heywang-Kobrunner SH, Beck R. Contrast-enhanced MRI of the breast. Berlin: Springer-Verlag; 1996.
2. Tofts PS, Berkowitz B, Schnall MD. Quantitative analysis of dynamic Gd-DTPA enhancement in breast tumors using a permeability model. Magn Reson Med 1995; 33:564–568.
3. Hoffmann U, Brix G, Knopp MV, Hess T, Lorenz WJ. Pharmacokinetic mapping of the breast: a new method for dynamic MR mammography. Magn Reson Med 1995;33:506–514.
4. Hulka CA, Smith BL, Sgroi DC, et al. Benign and malignant breast lesions: differentiation with echo-planar MR imaging. Radiology 1995;197:33–38.
5. den Boer JA, Hoenderop RK, Smink J, et al. Pharmacokinetic analysis of Gd-DTPA enhancement in dynamic three-dimensional MRI of breast lesions. J Magn Reson Imaging 1997;7:702–715.
6. van Dijke CF, Brasch RC, Roberts TP, et al. Mammary carcinoma model: correlation of macromolecular contrast-enhanced MR imaging characterizations of tumor microvasculature and histologic capillary density. Radiology 1996;198:813–818.
7. Daniel BL, Yen YF, Glover GH, et al. Breast disease—dynamic spiral MR imaging. Radiology 1998;209:499–509.
8. Brasch R, Pham C, Shames D, et al. Assessing tumor angiogenesis using macromolecular MR imaging contrast media. J Magn Reson Imaging 1997;7:68–74.
9. Buckley DL, Kerslake RW, Blackband SJ, Horsman A. Quantitative analysis of multi-slice Gd-DTPA enhanced dynamic MR images using an automated simplex minimization procedure. Magn Reson Med 1994;32:646–651.
10. Hawighorst H, Weikel W, Knapstein PG, et al. Angiogenic activity of cervical carcinoma—assessment by functional magnetic resonance imaging-based parameters and a histomorphological approach in correlation with disease outcome. Clin Cancer Res 1998;4:2305–2312.

11. Folkman J. What is the evidence that tumors are angiogenesis dependent? J Natl Cancer Inst 1990;82:4–6.
12. Knopp MV, Weiss E, Sinn HP, et al. Pathophysiologic basis of contrast enhancement in breast tumors. J Magn Reson Imaging 1999;10:260–266.
13. Passe TJ, Bluemke DA, Siegelman SS. Tumor angiogenesis: tutorial on implications for imaging. Radiology 1997;203:593–600.
14. Griebel J, Mayr NA, de Vries A, et al. Assessment of tumor microcirculation: a new role of dynamic contrast MR imaging. J Magn Reson Imaging 1997;7:111–119.
15. Tofts PS. Modeling tracer kinetics in dynamic Gd-DTPA MR imaging. J Magn Reson Imaging 1997;7:91–101.
16. Tofts PS, Brix G, Buckley DL, et al. Estimating kinetic parameters from dynamic contrast-enhanced T_1-weighted MRI of a diffusable tracer: standardized quantities and symbols. J Magn Reson Imaging 1999;10:223–232.
17. St Lawrence KS, Lee TY. An adiabatic approximation to the tissue homogeneity model for water exchange in the brain: I. Theoretical derivation. J Cereb Blood Flow Metab 1998;18:1365–1377.
18. Budinger TF, Huesman RH. Ten precepts for quantitative data acquisition and analysis. Circulation 1985;72(suppl IV):53–61.
19. Johnson JA, Wilson TA. A model for capillary exchange. Am J Physiol 1966;210:1299–1303.
20. Friedman MH. Principles and models of biological transport. Berlin: Springer-Verlag; 1986.
21. Adam G, Muhler A, Spuntrup E, et al. Differentiation of spontaneous canine breast tumors using dynamic magnetic resonance imaging with 24-gadolinium-DTPA-cascade-polymer, a new blood-pool agent. Preliminary experience. Invest Radiol 1996;31:267–274.
22. Demsar F, Shames DM, Roberts TPL, et al. Kinetics of MRI contrast agents with a size ranging between Gd-DTPA and albumin-Gd-DTPA: use of cascade-Gd-DTPA-24 polymer. Electro- Magnetobiol 1998;17:283–297.
23. Daldrup H, Shames DM, Wendland M, et al. Correlation of dynamic contrast-enhanced MR imaging with histologic tumor grade: comparison of macromolecular and small-molecular contrast media. AJR 1998;171:941–949.
24. Su MY, Wang Z, Carpenter PM, et al. Characterization of N-ethyl-N-nitrosourea-induced malignant and benign tumors in rats by using three MR contrast agents. J Magn Reson Imaging 1999;9:177–186.
25. Lassen NA, Perl W. Tracer kinetic methods in medical physiology. New York: Raven Press; 1979.
26. Crone C. The permeability of capillaries in various organs as determined by the use of the 'indicator dilution' method. Acta Physiol Scand 1963;58:292–305.
27. Renkin EM. Transport of potassium-42 from blood to tissue in isolated mammalian skeletal muscles. Am J Physiol 1959;197:1205–1210.
28. Lammertsma AA, Brooks DJ, Beaney RP, et al. In vivo measurement of regional cerebral haematocrit using positron emission tomography. J Cereb Blood Flow Metab 1984;4:317–322.
29. Wilson CB, Lammertsma AA, McKenzie CG, Sikora K, Jones T. Measurements of blood flow and exchanging water space in breast tumors using positron emission tomography: a rapid and noninvasive dynamic method. Cancer Res 1992;52:1592–1597.
30. Henderson E, Rutt BK, Lee TY. Temporal sampling requirements for the tracer kinetics modeling of breast disease. Magn Reson Imaging 1998;16:1057–1073.
31. Daldrup HE, Shames DM, Husseini W, et al. Quantification of the extraction fraction for gadopentetate across breast cancer capillaries. Magn Reson Med 1998;40:537–543.
32. Mussurakis S, Buckley DL, Drew PJ, et al. Dynamic MR imaging of the breast combined with analysis of contrast agent kinetics in the differentiation of primary breast tumours. Clin Radiol 1997;52:516–526.
33. Hulka CA, Edmister WB, Smith BL, et al. Dynamic echo-planar imaging of the breast: experience in diagnosing breast carcinoma and correlation with tumor angiogenesis. Radiology 1997;205:837–842.
34. Haase A. Snapshot FLASH MRI. Applications to T_1, T_2, and chemical-shift imaging. Magn Reson Med 1990;13:77–89.
35. Zur Y, Wood ML, Neuringer LJ. Spoiling of transverse magnetization in steady-state sequences. Magn Reson Med 1991;21:251–263.
36. Fritz-Hansen T, Rostrup E, Larsson HB, et al. Measurement of the arterial concentration of Gd-DTPA using MRI: a step toward quantitative perfusion imaging. Magn Reson Med 1996;36:225–231.
37. Tsekos NV, Zhang Y, Merkle H, et al. Fast anatomical imaging of the heart and assessment of myocardial perfusion with arrhythmia insensitive magnetization preparation. Magn Reson Med 1995;34:530–536.
38. Jerosch-Herold M, Wilke N, Stillman AE. Magnetic resonance quantification of the myocardial perfusion reserve with a Fermi function model for constrained deconvolution. Med Phys 1998;25:73–84.
39. Brix G, Schad LR, Deimling M, Lorenz WJ. Fast and precise T_1 imaging using a TOMROP sequence. Magn Reson Imaging 1990;8:351–356.
40. Zheng J, Venkatesan R, Haacke EM, et al. Accuracy of T_1 measurements at high temporal resolution: feasibility of dynamic measurement of blood T_1 after contrast administration. J Magn Reson Imaging 1999;10:576–581.
41. McKenzie CA, Pereira RS, Prato FS, Chen Z, Drost DJ. Improved contrast agent bolus tracking using T_1 FARM. Magn Reson Med 1999;41:429–435.
42. Tadamura E, Hatabu H, Li W, Prasad PV, Edelman RR. Effect of oxygen inhalation on relaxation times in various tissues. J Magn Reson Imaging 1997;7:220–225.
43. Noseworthy MD, Kim JK, Stainsby JA, Stanisz GJ, Wright GA. Tracking oxygen effects on MR signal in blood and skeletal muscle during hyperoxia exposure. J Magn Reson Imaging 1999;9:814–820.
44. Donahue KM, Burstein D, Manning WJ, Gray ML. Studies of Gd-DTPA relaxivity and proton exchange rates in tissue. Magn Reson Med 1994;32:66–76.
45. Seber GAF, Wild CJ. Nonlinear regression. New York: John Wiley & Sons; 1989.
46. Gowland PA, Leach MO. Fast and accurate measurements of T_1 using a multi-readout single inversion-recovery sequence. Magn Reson Med 1992;26:79–88.
47. Parker GJ, Suckling J, Tanner SF, et al. RIW: parametric analysis software for contrast-enhanced dynamic MR imaging in cancer. Radiographics 1998;18:497–506.
48. Cron GO, Santyr G, Kelcz F. Accurate and rapid quantitative dynamic contrast-enhanced breast MR imaging using spoiled gradient-recalled echoes and bookend T_1 measurements. Magn Reson Med 1999;42:746–753.
49. Mottolese M, Morelli L, Agrimi U, et al. Spontaneous canine mammary tumors. A model for monoclonal antibody diagnosis and treatment of human breast cancer. Lab Invest 1994;71:182–187.
50. Raynaud JP, Cotard M, Andre F, et al. Spontaneous canine mammary tumour: a model for human endocrine therapy? J Steroid Biochem 1981;15:201–207.
51. Gilbertson SR, Kurzman ID, Zachrau RE, Hurvitz AI, Black MM. Canine mammary epithelial neoplasms: biologic implications of morphologic characteristics assessed in 232 dogs. Vet Pathol 1983;20:127–142.
52. Evelhoch JL. Key factors in the acquisition of contrast kinetic data for oncology. J Magn Reson Imaging 1999;10:254–259.
53. Lee TY, Henderson E, Rutt BK. Temporal sampling requirements for the estimation of blood flow, blood volume and extraction ratio from dynamic contrast-enhanced MRI studies (abstract). In: Proceedings of the ISMRM 8th Annual Meeting, 2000. p 621.
54. Eskey CJ, Koretsky AP, Domach MM, Jain RK. ^{2}H nuclear magnetic resonance imaging of tumor blood flow: spatial and temporal heterogeneity in a tissue-isolated mammary adenocarcinoma. Cancer Res 1992;52:6010–6019.
55. Less JR, Skalak TC, Sevick EM, Jain RK. Microvascular architecture in a mammary carcinoma: branching patterns and vessel dimensions. Cancer Res 1991;51:265–273.
56. Berkowitz BA, Tofts PS, Sen HA, Ando N de JE Jr. Accurate and precise measurement of blood-retinal barrier breakdown using dynamic Gd-DTPA MRI. Investigative Ophthalmol Vis Sci 1992;33:3500–3506.
57. Larson KB, Markham J, Raichle ME. Tracer-kinetic models for measuring cerebral blood flow using externally detected radiotracers. J Cereb Blood Flow Metab 1987;7:443–463.

58. Henderson E. Temporal sampling and signal-to-noise ratio requirements for the aaJW model. In: Measurement of blood flow, blood volume and capillary permeability in breast tumours using contrast-enhanced magnetic resonance imaging (PhD thesis), The University of Western Ontario, London, Canada, 1999. p 88–102.
59. Donahue KM, Weisskoff RM, Burstein D. Water diffusion and exchange as they influence contrast enhancement. J Magn Reson Imaging 1997;7:102–110.
60. Judd RM, Reeder SB, May-Newman K. Effects of water exchange on the measurement of myocardial perfusion using paramagnetic contrast agents. Magn Reson Med 1999;41:334–342.
61. Vaupel P. Tumor blood flow. In: Molls M, Vaupel P, editors. Blood perfusion and microenvironment of human tumors: implications for clinical radiooncology, vol 1. Berlin: Springer-Verlag; 1998. p 41–45.
62. Jain RK. Determinants of tumor blood flow: a review. Cancer Res 1988;48:2641–2658.
63. Peterson HI, Appelgren L, Lundborg G, Rosengren B. Capillary permeability of two transplantable rat tumours as compared with various normal organs of the rat. Bibl Anat 1973;12:511–518.
64. Tong CY, Prato FS, Wisenberg G, et al. Measurement of the extraction efficiency and distribution volume for Gd-DTPA in normal and diseased canine myocardium. Magn Reson Med 1993;30:337–346.
65. Howard-Lech VL, Lee TY, Craen RA, Gelb AW. Cerebral blood volume measurements using dynamic contrast-enhanced x-ray computed tomography: application to isoflurane anaesthetic studies. Physiol Meas 1999;20:75–86.
66. Freeman AJ, Gowland PA, Mansfield P. Optimization of the ultrafast Look-Locker echo-planar imaging T_1 sequence. Magn Reson Imaging 1998;16:765–772.